High-temperature creep resistant ternary blends based on polyethylene and polypropylene for thermoplastic power cable insulation

(article starts on next page)

RESEARCH ARTICLE

Ion transport and relaxation in phosphonium poly(ionic liquid) homo- and co-polymers

Palash Banerjee[1] | Pulak Pal[1] | Aswini Ghosh[2] | Tarun K. Mandal[1]

[1]School of Chemical Sciences, Indian Association for the Cultivation of Science, Jadavpur, Kolkata, India

[2]School of Physical Sciences, Indian Association for the Cultivation of Science, Jadavpur, Kolkata, India

Correspondence
Tarun K. Mandal, School of Chemical Sciences, Indian Association for the Cultivation of Science, Jadavpur, Kolkata 700032, India.
Email: psutkm@iacs.res.in

Abstract

In the present work, a poly(ionic liquid) (PIL), poly(triphenyl-4-vinylbenzylphosphonium chloride) and a series of its random copolymers with nonionic hydrophobic poly(methyl methacrylate) (PMMA) are synthesized by conventional free radical polymerization (CFRP) and reversible addition-fragmentation chain-transfer (RAFT) polymerization. The understanding of some fundamental aspects about ion transport and relaxation mechanism in PIL and PIL copolymers are investigated using dielectric spectroscopy via several theoretical models. The influence of copolymer compositions, physical blending of neat PIL and PMMA, size of counter anions (Cl^- and $TFSI^-$) and variation of molecular weights on thermal stability, moisture sensitivity, ionic transport and relaxation properties are also studied. An enhancement of thermal stability and ionic transport property of the PIL copolymer is observed compared to those of the physically mixed blend of two homopolymers with same compositions. The incorporation of hydrophobic PMMA segment definitely decreases the moisture content in PIL copolymers than the PIL itself. In all these PIL- based systems, the temperature dependence of ionic conductivity, relaxation time and ion diffusivity are well described by Vogel-Tammann-Fulcher model. The studies of some fundamental properties of these new PIL copolymers with less moisture sensitivity may help in using them as potential polymer electrolytes in energy storage devices.

KEYWORDS

copolymer, dielectric spectroscopy, ion transport, ionic conductivity, poly(ionic liquid)

1 | INTRODUCTION

In recent years, a number of significant efforts have been made by the materials scientists to develop advanced functional materials to overcome the challenges in efficient energy storage and its utilization.[1–6] Recently, polymerized ionic liquids (PILs) have received significant attention for their use as solid polymer electrolytes in several energy storage and conversion devices such as lithium-ion batteries, dye-sensitized solar cells, supercapacitors, fuel cells, etc.[7–11] Actually, PILs belong to an interesting subclass of polymer electrolytes containing an ionic liquid (IL) species in each of the monomer unit that constitutes the polymer backbone. Thus, PILs are also known as single ion conductors as they have non-conducting ions bound to the polymer backbone/side chain, while the counter ions conduct because of their mobile nature.[12–17] Fundamentally, the molecular level understanding of the charge carrier transport mechanism and relaxation in these types of ionic polymers are needed for rational designing of PILs for electrochemical applications.[13] However, the low ionic conductivity of

polymer electrolytes at room temperature limits their applications in electrochemical devises. Therefore, it is highly important to have a clear understanding of the fundamental parameters[1,14,15,18,19] and how several factors such as chemical structure, morphologies, etc. influence the ion transport mechanism in PIL systems. However, many of such reported studies remain controversial and require further exploration.

As per the Nernst-Einstein relation, $\sigma = \sum p_i q_i \mu_i$, the ionic conductivity (σ) of a liquid electrolyte is strongly controlled by the ion mobility (μ_i) (inversely proportional to ion diffusivity) and free ion number density (p_i).[20,21] Furthermore, the ion diffusivity in liquid electrolyte is largely controlled by medium viscosity (η) and structural relaxation time (τ_s). As reported in the literature, the classical mechanics assumes a strong coupling of charge carrier diffusion to structural relaxation (viscosity) for liquid electrolyte.[22] A similar mechanism has also been proposed for polymer electrolytes by different groups, where the charge carrier dynamics (diffusion) depends on local segmental motion of polymer chain.[23,24] In particular, in the cases of superionic glasses or crystal systems, a faster ion dynamics have been observed even in frozen condition of segmental dynamics, resulting in high ionic conductivity compared to ideal coupled system.[25,26] A similar decoupling of the charge carrier transport from segmental dynamics has also been reported for several PILs.[19,27–29] It is hypothesized that the frustration in chain packing in PIL can cause such decoupling phenomenon.[1] Ultimately, the decoupling of ion dynamics from segmental motion is the most promising approach to achieve high ionic conductivity in polymer electrolytes at room temperature. Moreover, there have been a series of studies to examine the effect of tuning of cation/anion size,[30,31] position of ions (either in the main chain or in the side chain) of PIL,[19,29,32,33] variation of molecular weight,[18] changing the space between neighboring PIL chains,[13] pressure exerted during conductivity measurement,[1] variation of chain length,[34] glass transition temperature (T_g),[14,30,35] chain polarity,[36] etc., on the change of ionic transport in PIL systems. Dielectric spectroscopic (DS) technique is reported to be the most popular method to investigate ionic conductivity, ion transport and relaxation mechanism in electrolyte systems.[29,37–39] However, such studies have been reported for only limited number of PILs which are mostly homopolymers. In particular, there are a very limited number of studies done on ion conduction in PIL-based copolymers. From the energy storage application point of view, the copolymers of PIL and hydrophobic polymer are of great importance because they are expected to be less moisture sensitive. Therefore, the exploration of ion transport properties in such type of PIL copolymers is necessary for their futuristic application in electrochemical devices.

Thus, this work is focused on the studies of ion transport and relaxation in PIL homo- and co-polymers as single ion conducting polymeric electrolytes using dielectric spectroscopy. In particular, this study puts special emphasis on examining how the composition of PIL copolymer, nature of counter anion and molecular weight (M_n) affects the ion transport properties in these PIL-based systems. For comparison, similar studies are also conducted on materials obtained by physical mixing of PIL and hydrophobic poly(methyl methacrylate) (PMMA) that actually constitute the copolymer. To do such experiment, poly(triphenyl-4-vinylbenzylphosphonium chloride) (P[VBTP][Cl]) homopolymer and a series of P[VBTP][Cl]-*ran*-PMMA PIL copolymers of varying compositions are synthesized by conventional free radical polymerization. Another series of PIL copolymers with varying molecular weights were also synthesized by reversible addition-fragmentation chain-transfer (RAFT) polymerization technique. This work further demonstrates that it is possible to enhance the thermal stability and electrical properties of the PIL copolymers compared to the physically mixed blend of two constituent polymer segments.

2 | EXPERIMENTAL

2.1 | Materials

Methyl methacrylate (MMA, >99%), 4-vinylbezyl chloride (VBC, 90%), 2′-azobis(2-methylpropionitrile) (AIBN, 98%), 4-cyano-4-[(dodecylsulfanylthiocarbonyl) sulfanyl] pentanoic acid (CDP, ≥ 97%) and bis(trifluoromethane)-sulfonimide lithium salt (LiTFSI, >99%) were used as purchased from Sigma-Aldrich. Triphenylphosphene (TPP) was obtained from TCI chemicals. Dimethylformamide (DMF) was received from Merck, India. MMA and VBC monomers were passed through alumina columns for removal of inhibitors. AIBN and TPP were recrystallized twice from ethanol prior to use. DMF was kept overnight with anhydrous $CaCl_2$ and distilled over CaH_2 under reduced pressure prior to use. Milli-Q water was used in the preparation of various solutions.

2.2 | Synthesis of different random PIL copolymers

A series of random PIL copolymers [P[VBTP][Cl]-*ran*-PMMA copolymers (**P1**-**P3**)] (Table 1) of varying

TABLE 1 Polymerization conditions and molecular characterization data of P[VBTP][Cl] and different P[VBTP][Cl] based systems

PIL systems[a]	$[M_1:M_2]_o$:$[CDP]_o$:$[AIBN]_o$	M_n (SEC) (kDa)	M_p (MALDI-TOF MS) (kDa)	Đ (SEC)	Ionic content (IC)[e] (wt%)
P[VBTP][Cl]	[100:0]:00:2	23.3	–	1.65	100
P[VBTP][Cl]$_{20}$-*ran*-PMMA$_{80}$ (P1)	[20:80]:00:2	28.9	–	1.92	18
P[VBTP][Cl]$_{50}$-*ran*-PMMA$_{50}$ (P2)	[50:50]:00:2	20.15	–	1.56	24.7
P[VBTP][Cl]$_{80}$-*ran*-PMMA$_{20}$ (P3)	[80:20]:00:2	19.1	–	1.69	88.34
P[VBTP][TFSI]$_{80}$-*ran*-PMMA$_{20}$ (P4)	[80:20]:00:2	19.1	–	1.69	88.34
P[VBTP][Cl]$_{80}$-*ran*-PMMA$_{20}$-6.2k[b] (P5)	[80:20]:1:0.2	6.2	–	1.20	89.1
P[VBTP][Cl]$_{80}$-*ran*-PMMA$_{20}$-2.4k[c] (P6)	[80:20]:10:2	–[d]	2378	–	50
P[VBTP][Cl]$_{80}$-*ran*-PMMA$_{20}$-1.4k[c] (P7)	[80:20]:20:4	–[d]	1391	–	66
PMMA	[00:100]:00:2	25.48	–	1.79	00

Note: Reaction condition: Time = 24 h; Temperature = 65°C; Solvent = DMF; M_1 = [VBTP][Cl]; M_2 = MMA; Monomer concentration = 10 wt%. P5-P7 were the samples of molecular weights 6.2, 2.4 and 1.4 kDa respectively. P8 and P9 were the physical blends of P[VBTP][Cl] and PMMA homopolymers with a ratio of 1:4 and 4:1 (wt/wt) respectively.

[a]The numerical value represents the feed ratios of the comonomers.

[b]Molecular weight obtained from SEC (Figure S11).

[c]Molecular weight obtained from MALDI-TOF Mass Spectrometry (Figures S12,S13).

[d]Not measurable.

[e]Obtained from ^{1}H-NMR spectral analysis.

compositions were prepared from triphenyl-4-vinylbenzylphosphonium chloride ([VBTP][Cl]) ionic liquid monomer (ILM) and hydrophobic MMA monomer by conventional free radical polymerization (CFRP) using AIBN as the initiator (Scheme 1). The anion-exchange of chloride ion of **P3** (P[VBTP][Cl]$_{80}$-*ran*-PMMA$_{20}$) by bis(trifluoromethane) sulfonamide (TFSI$^-$) ion was done using a reported protocol[40] as shown in Scheme 1. The obtained ion exchanged copolymer was designated as **P4** (Table 1). The reversible addition-fragmentation chain-transfer (RAFT) polymerization technique using CDP as the chain transfer agent and AIBN as initiator respectively was also used to synthesize low molecular weight copolymers (**P5-P7**, Table 1) (Scheme 1). The detailed reaction recipe and the synthesis protocol are provided in the Supporting Information. Note that the synthesis protocol and the detailed characterization of the [VBTP][Cl] monomer was described in our earlier paper.[41]

*Homopolymers P[VBTP][Cl] and PMMA are synthesized by the CFRP method using [VBTP][Cl] and MMA respectively as monomer and AIBN as initiator.

2.3 | Synthesis of homopolymers (P[VBTP][cl] and PMMA)

P[VBTP][Cl] and PMMA were also synthesized separately by the same procedure as used for **P1 (**see SI**)** at a concentration of 10 wt% of [VBTP][Cl] and MMA monomers respectively using AIBN as the initiator.

2.4 | Preparation of binary blends [P[VBTP][Cl]/PMMA(20/80) (P8) and P[VBTP][Cl]/PMMA(80/20) (P9)]

The blends of P[VBTP][Cl] and PMMA were prepared by solution-casting method. Two blend samples **P8** and **P9** were prepared by weighing P[VBTP][Cl] (M_n = 23.3 kDa) and PMMA (M_n = 25.5 kDa) in the ratios of 1:4 and 4:1 (w/w) respectively. Each sample mixture was then dissolved in DMF at a concentration of 5 wt% and vigorously stirred at 60 °C overnight to form a homogeneous mixture. The blend samples were then isolated by precipitation in diethyl ether followed by drying overnight in vacuum oven at 70 °C and collected as white powder.

2.5 | Characterizations

^{1}H-NMR spectra of all the homopolymers and copolymers (Figure S1-S9) and ^{19}F-NMR spectrum of **P4** (Figure S10) were recorded on a Bruker DPX 500 MHz spectrometer (see SI for details). SEC technique was utilized to determine the number average molecular weights (M_ns) and dispersities (Đs) of copolymers and homopolymers using a Waters GPC system connected with three Styragel columns (see SI). The thermogravimetric analysis (TGA) and differential scanning calorimetry (DSC) of all the PIL systems were done using TGA instrument (TA, model Q50) and DSC instrument (Q2000, TA instrument) respectively (see SI). Field emission scanning
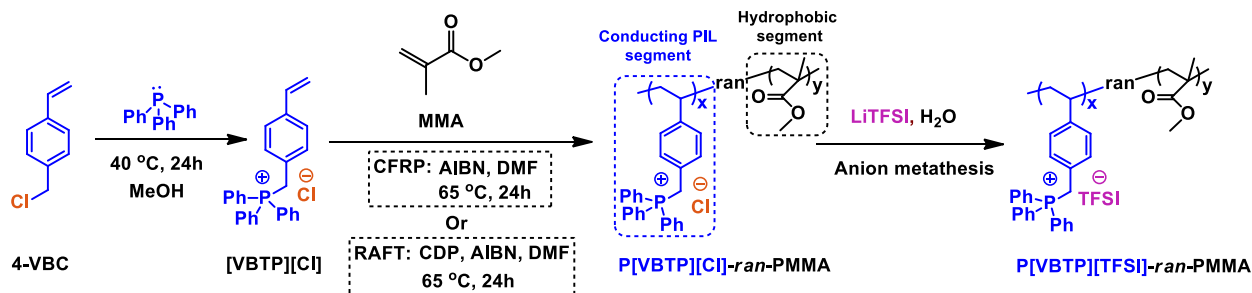
SCHEME 1 Synthetic scheme for synthesis of (A) P[VBTP][Cl]-*ran*-PMMA random copolymers via CFRP or RAFT polymerization and (B) P[VBTP][TFSI]-*ran*-PMMA copolymer by anion metathesis of the chloride to bis(trifluoromethane)sulfonamide (TFSI⁻) ion [Color figure can be viewed at wileyonlinelibrary.com]

electron microscope (FESEM) images of different samples were taken from JEOL FESEM (Model: JSM 7500F) at an accelerating voltage 5 kV (see SI for details). Matrix-assisted laser desorption/ionization time of flight (MALDI-TOF-MS) spectra were acquired in a Brucker instrument (Applied Biosystems) to determine the molecular weights of **P6** and **P7** (see SI for details of sample preparation). The dielectric spectroscopic (DS) measurement of samples at different temperatures was carried out using an LCR spectrometer (HIOKI, model: IM 3536) in the frequency range of 4 Hz - 8 MHz with a perturbation potential of 1.0 V (see SI).

2.5.1 | Determination of saturated water content in PIL systems

To access the applicability of PIL systems, we have determined the saturated water content in the samples. Thus, to measure the saturated water content in PIL systems, typically, a sample and a water-filled beaker were kept inside a desiccator for 7 days for allowing the sample to absorb maximum amount of moisture. The water content was then estimated from weight loss in TGA thermogram of the respective water-absorbed samples at and above 100 °C.

3 | RESULTS AND DISCUSSION

3.1 | Synthesis and characterization of PIL homo- and Co-Polymers

The synthesis of PIL, P[VBTP][Cl] and its copolymers were achieved either by CFRP or RAFT techniques as shown in Scheme 1. The counter anion exchange of the Cl⁻ ion of **P3** (Table 1) with bis(trifluoromethane)sulfonamide (TFSI⁻) ion to **P4** is also shown in Scheme 1. The chemical compositions of PIL copolymers were

determined from the analysis of ^{1}H NMR spectra (Figures S1-S9 in SI for details) and are summarized in Table 1. ^{19}F NMR spectra of **P4** (Figure S10) were recorded relative to neat hexafluorobenzene (C_6F_6) at −164.9 ppm and the distinct signal at 81.02 ppm clearly referred to the presence of TFSI⁻ anions in the copolymer. To confirm the absence of Cl⁻ ion in **P4**, 50 mg of this copolymer was first leached with 1 mL of water followed by the drop wise addition of 1 M aqueous AgNO$_3$ solution in the presence of excess dilute nitric acid. No white precipitate of AgCl was observed in this experiment, which confirmed the absence of any free Cl⁻ ion in copolymer **P4**. The comparison of ^{1}H-NMR spectra of copolymer before (**P3**) and after exchange (**P4**) (Figure S14) clearly revealed a shift of signal of methylene protons adjacent to phosphonium cation from δ 5.32 to 5.02 ppm providing further evidence of exchange of Cl⁻ with TFSI⁻ ion.
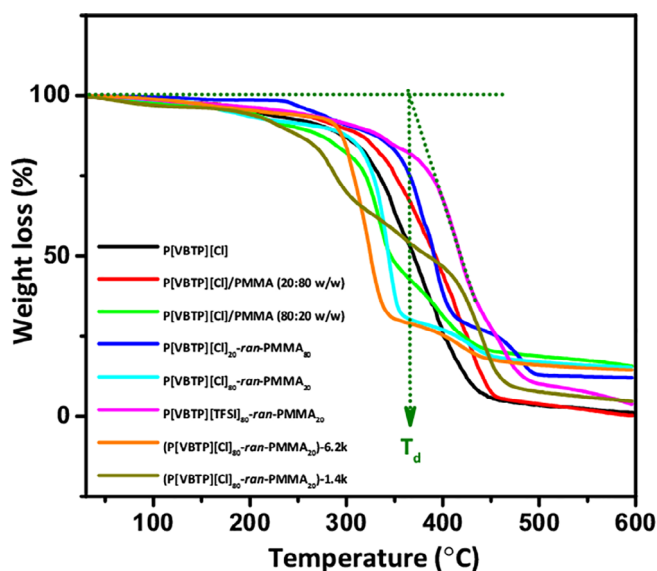
3.2 | Thermal properties

PIL with higher thermal stability is one of the key factors for its application as an energy storage material. Figure 1 presents the TGA traces of different PIL systems (Table 1). Generally, the decomposition temperature (T_d) in TGA is controlled by chemical structure of PIL backbone.[42] The values of T_d of different PIL systems were listed in Table 2. We did not measure the thermal stability of samples **P2** and **P7** by TGA as the major conclusion can be drawn without the analysis of these two samples. It can be seen from Table 2 that the PIL copolymers (**P1** and **P3**) showed high decomposition temperature over 316 °C than those of the neat P[VBTP][Cl] as well as physically mixed blends of P[VBTP][Cl] and PMMA (**P8** and **P9**). The decomposition temperature is increased with increase of non-ionic methyl methacrylate (MMA) hydrophobic polymer segment in homo-PIL. On the other hand, the P[VBTP][TFSI]$_{80}$-*ran*-PMMA$_{20}$ (**P4**)

showed higher value of T_d compared to that of P[VBTP][Cl]$_{80}$-ran-PMMA$_{20}$ (**P3**) and indicated that the exchange of anion influences the thermal stability (Table 2). The enhancement of thermal stability of PIL copolymer with TFSI⁻ ion has been attributed to the higher nucleophilicity of TFSI⁻ ion.[43] As expected, Figure 1 also reveals that the thermal stability decreases with the decrease of M_n of PIL copolymers (**P5** and **P7**) (Table 2).

Moreover, the high thermal stabilities of PIL copolymers enable them to use in high temperature electrochemical operation for energy storage applications such as Li-ion batteries, etc. We have also measured the thermal stability of PMMA and PIL systems after their complete exposure under saturated water vapor as shown in Figure S15. It was also observed from Figure S15 that the thermal stability of copolymers is still better than that of homo PIL after saturated amount of moisture absorption. The saturated water content of PMMA and different PIL systems such as PMMA, P[VBTP][Cl], **P1**, **P2**, **P3**, **P4**, **P7**, **P8** and **P9** were measured to be 0.24, 12.80, 1.13, 4.86, 6.41, 1.84, 10.45, 1.15 and 3.35 respectively. We found that the copolymers contain less amount of water than that of homopolymer due to the presence of hydrophobic PMMA segment in the copolymer. It should be noted that no glass transition temperature of the PIL copolymers could be detected by DSC (Figure S16). We have also measured the glass transition temperature for copolymers of other compositions and got similar results.

3.3 | Dielectric spectra of PIL based systems

Figure 2 presents a typical example of different representative forms of dielectric spectra for P[VBTP][Cl] at a temperature of 333 K. The dielectric constant $\varepsilon'(\omega)$ (orange), dielectric loss $\varepsilon''(\omega)$ (pink) and derivative dielectric loss spectra (ε''_{der}) (green) of P[VBTP][Cl] are given in Figure 2(A). The derivative of loss spectra ε''_{der} [= $(-\pi/2) \times (\partial\varepsilon'/\partial ln\omega)$] based on Kramers-Kronig relation can reveal all other relaxation, which are actually suppressed by conductivity relaxation process.[44,45] On the other hand, according to linear response theory, the complex dielectric spectroscopy, $\varepsilon^*(\omega)$ can be represented in terms of complex conductivity spectroscopy $\sigma^*(\omega)$ and complex electric modulus spectroscopy $M^*(\omega)$ that are related by the following expression:

$$M^*(\omega) = [M'(\omega) + iM''(\omega)] = 1/\varepsilon^*(\omega) = i\omega\varepsilon_0/\sigma^*(\omega)$$
$$= i\omega\varepsilon_0/[\sigma'(\omega) - i\sigma''(\omega)],$$

FIGURE 1 Thermogravimetric analysis (TGA) traces of different PIL systems [Color figure can be viewed at wileyonlinelibrary.com]

TABLE 2 Decomposition temperature (T_d), ionic conductivity at 303 K and power law exponent n at 333 K for the PIL and PIL based systems

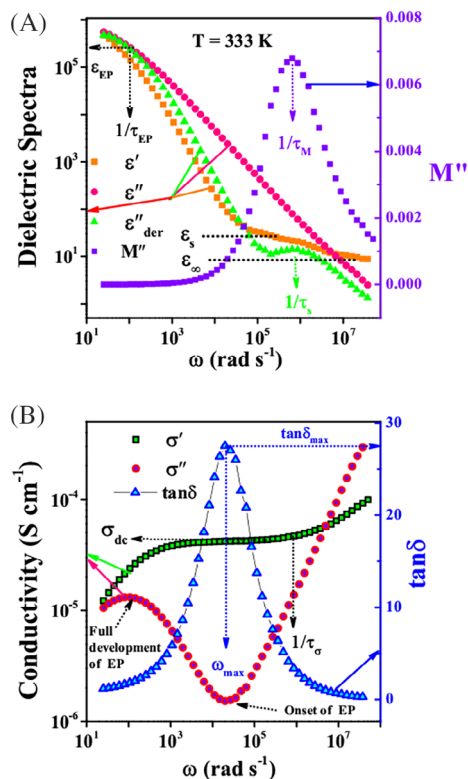| PIL systems	T_d (°C) (±4)	σ_{dc} (S cm⁻¹)	n (±0.04)
P[VBTP][Cl]	301	1.96×10^{-6}	0.57
P[VBTP][Cl]$_{20}$-ran-PMMA$_{80}$(**P1**)	352	4.24×10^{-9}	0.62
P[VBTP][Cl]$_{50}$-ran-PMMA$_{50}$(**P2**)	NM	4.78×10^{-8}	0.55
P[VBTP][Cl]$_{80}$-ran-PMMA$_{20}$(**P3**)	316	1.95×10^{-7}	0.56
P[VBTP][TFSI]$_{80}$-ran-PMMA$_{20}$(**P4**)	365	2.96×10^{-8}	0.61
P[VBTP][Cl]$_{80}$-ran-PMMA$_{20}$-6.2 k(**P5**)	288	1.77×10^{-5}	0.58
P[VBTP][Cl]$_{80}$-ran-PMMA$_{20}$-2.4 k(**P6**)	NM	2.56×10^{-5}	0.56
P[VBTP][Cl]$_{80}$-ran-PMMA$_{20}$-1.4 k(**P7**)	265	3.73×10^{-5}	0.54
P[VBTP][Cl]/PMMA (20:80 w/w) (**P8**)	324	5.32×10^{-11}	0.65
P[VBTP][Cl]/PMMA (80:20 w/w) (**P9**)	278	1.48×10^{-7}	0.58

Abbreviation: NM, not measured.

FIGURE 2 Dielectric spectroscopic data in several representations for P[VBTP][Cl]: (A) dielectric constant (ε') (orange solid squares), dielectric loss (ε'') (pink solid circles), derivative of dielectric loss (ε''_{der}) (green solid triangles) and modulus loss (M'') (violet diamonds) and (B) real part of complex conductivity (σ') (black open squares), imaginary part of complex conductivity (σ'') (red open circles) and loss tangent ($\tan\delta$) (blue open triangles) [Color figure can be viewed at wileyonlinelibrary.com]

where $\sigma'(\omega)$ and $\sigma''(\omega)$ are real and imaginary part of the complex conductivity respectively and $M'(\omega)$ and $M''(\omega)$ respectively are real and imaginary part of complex electric modulus. The M'' (imaginary part of M^* response) of P[VBTP][Cl] is shown in Figure 2(A). The real $\sigma'(\omega)$, imaginary $\sigma''(\omega)$ parts of the complex conductivity and $\tan\delta$ are also displayed in Figure 2(B) as a function of angular frequency ($\omega = 2\pi f$). The dielectric permittivity spectra of P[VBTP][Cl] showed three major mutually correlated phenomena: (i) electrode polarization (EP), (ii) dc conductivity and (iii) dielectric relaxation process in the low, medium and high frequency region respectively. A huge increase of dielectric constant (ε'), dielectric loss (ε'') and derivative spectra (ε''_{der}) with decreasing angular frequency including a small plateau in low frequency region was observed due to the formation of a space charge layer by the accumulation of charge carrier near metallic blocking electrodes (Figure 2(A)). Actually, the quick voltage drops due to the absence of ion drift in this region creates a large EP of the materials. This response

was also reflected in real and imaginary parts of the conductivity spectroscopy and the value of conductivity decreased with decreasing angular frequency in the low frequency region as can be seen clearly in Figure 2(B).[46] Generally, EP is an extrinsic and non-equilibrium phenomenon. It is directly linked to charge carrier dynamics as well as dependent on the thickness of the specimen, nature of the electrode interface and type of material of the electrode.[47,48] As shown in Figure 2(A), a sharp increase in values ε' and ε''_{der} was observed at a certain angular frequency where the EP effect began corresponding to a minimum in the imaginary part [$\sigma''(\omega)$] of complex conductivity (Figure 2(B)). Such angular frequency (ω) was denoted as ω_{on} corresponding to onset of the EP process, i.e., ions reached the metal electrode and began to accumulate on the electrode surface. The full development of EP in the specimen occurred at a certain angular frequency, ω ω_{max}, corresponding to a peak in imaginary part, $\sigma''(\omega)$ of complex conductivity where a slope in dielectric constant ($\varepsilon'(\omega)$) started towards low frequency in dielectric permittivity (Figure 2(A)). A frequency independent plateau region (Figure 2(B)) was observed in the mid frequency region of $\sigma'(\omega)$ corresponding to ionic conductivity of the material representing long-range ion diffusion through successive hopping process from one favorable site to other neighboring site in a polymer network. A shoulder/plateau like feature (Figure 2(A)) was also observed in $\varepsilon'(\omega)$ in the same frequency region. Any value of dielectric constant in this region was denoted as static dielectric constant (ε_s), which is linked with long range ion hopping process. A leveling off is observed in the PILs under applied electric field towards the higher frequency region which is denoted as ε_∞ (high frequency limit value) in $\varepsilon'(\omega)$. However, the corresponding conductivity value significantly increased with the increase of frequency due to dipolar relaxation in the high frequency region, which is denoted as frequency dispersive region (Figure 2(B)). In spite of having bulk characteristics and EP features, the dielectric loss data sharply decreased with the increase of frequency (Figure 2(A)). However, ε''_{der} showed a prominent peak at high frequency region corresponding to segmental relaxation time (τ_s) of polymer chain as suggested by other research groups.[27] On the other hand, a crossover region, where a jump from frequency independent region to dispersive region occurred, is generally known as the onset of the so-called hopping regime and hopping frequency can be denoted as $\omega_H = 1/\tau_H = 1/\tau_\sigma = \varepsilon_s\varepsilon_0/\sigma_0$, ε_0 ($= 8.85 \times 10^{-12}$ F m^{-1}) is the dielectric permittivity of free space.[47,49] Alternatively, the dielectric spectra can be appropriately analyzed in terms of electric modulus, in which EP is suppressed at low frequency regime. As shown in Figure 2(A), electric modulus loss $M''(\omega)$

displayed a long tail in low frequency region associated with large capacitance due to the electrode-electrolyte interface and a distinct peak related with a transition from long to short range ionic motion. Such peak is correlated to the conductivity relaxation.[50] The time when diffusions of ions start is known as conductivity relaxation time (τ_M).[35] It should be noted that peak maxima in $\varepsilon''_{der}(\omega)$ response, conductivity relaxation in $M''(\omega)$ response and hopping frequency (ω_H) in conductivity response are very close to each other and also provide vital information for the origin of the dielectric relaxation peak. The peak maximum (ω_{max}) in frequency dependence of $tan\delta$ curve was situated at the onset of EP response (Figure 2(B)). The mobile ion diffusivity and number density can be estimated using the value of $tan\delta_{max}$ and ω_{max} obtained from $tan\delta$ spectroscopy employing the Macdonald-Trukhan model.[51–53] It is worth to mention that the diffusivity and number density of ions in electrolyte materials can also be estimated from this model, which are usually over estimated compared to that obtained from the PFG-NMR technique.[54] However, several authors have calculated the diffusivity and ion density using the physical model proposed by the Macdonald-Coelho, which agreed well with the value obtained from the PFG-NMR.[35,55,56]
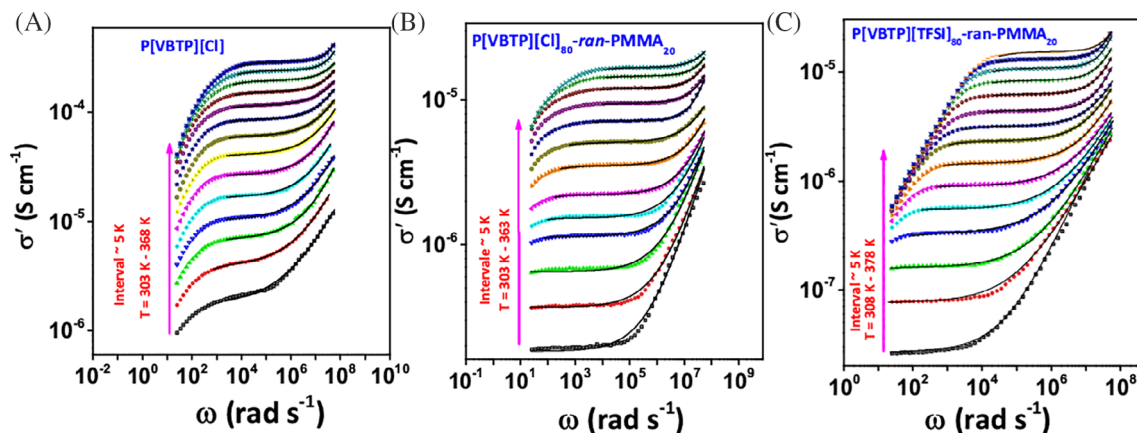
3.4 | Analysis of conductivity spectra

The real $\sigma'(\omega)$ part of complex conductivity $\sigma^*(\omega)$ spectra of the P[VBTP][Cl], P[VBTP][Cl]$_{80}$-ran-PMMA$_{20}$ and P[VBTP][TFSI]$_{80}$-ran-PMMA$_{20}$ in the frequency range of 4 Hz–8 MHz at different temperatures are presented in Figure 3. The conductivity spectroscopy is often analyzed by using several physical model such as

universal power law (UPL) model based on non-uniform hopping distance with multidimensional arbitrarily varying potential barriers,[57] random barrier model (RBM) based on the uniform hopping distance with equal potential landscape,[58] etc. Actually, ions transport in polymer electrolyte occurs via hopping of ions from one favorable site to other site in intra- and inter-polymer chains and also thermal motion of polymeric chains.[59] Due to thermal chain dynamics, a new favorable position is created by destroying their old accessible position in polymeric network. Thus, polymeric system represents a media where exists a non-uniform hopping distance with arbitrary potential landscape. There is a restriction of RBM applicability frequency range near dc to ac conductivity transition and significant deviations exist between model predictions and experimental data. The RBM is unable to describe the whole conductivity spectra of these PIL materials. Thus, it is appropriate to analyze the conductivity spectra using UPL model.[38] At first, the conductivity spectra of P[VBTP][Cl] (Figure 3(A)) were analyzed using UPL model,[57,60] as it is the best for describing polymer electrolyte systems. According to UPL model, the real conductivity $\sigma'(\omega)$ can be expressed in terms of dc conductivity σ_{dc} and hopping (diffusion) rate of ion ω_H ($\sim 1/\tau_H$) as

$$\sigma'(\omega) = \sigma_{dc}\left[1 + \left(\frac{\omega}{\omega_H}\right)^n\right], \qquad (1)$$

where n is an exponent ($0 < n \leq 1$), related to interactions between mobile ions and dimensionality of conduction pathway.[61] However, this relation is not applicable for materials with EP effect in low-frequency region at relatively high temperatures. Figure 3(A) shows the fitting of the real part $\sigma'(\omega)$ of complex conductivity

FIGURE 3 Real $\sigma'(\omega)$ part of complex conductivity spectra of P[VBTP][Cl] (A), P[VBTP][Cl]$_{80}$-ran-PMMA$_{20}$ (B) and P[VBTP][TFSI]$_{80}$-ran-PMMA$_{20}$ (C) respectively in the frequency ranges from 4 Hz- 8 MHz at different temperatures. The black lines in Figures 3(A)–(C) were fitted to Equation 1 [Color figure can be viewed at wileyonlinelibrary.com]

spectra in the dispersive region to Equation 1. The analyses of conductivity spectra of P[VBTP][Cl]$_{80}$-*ran*-PMMA$_{20}$ (Figure 3(B)) and P[VBTP][TFSI]$_{80}$-*ran*-PMMA$_{20}$ (Figure 3(C)) can also be done by applying the same UPL model as used for neat P[VBTP][Cl] (Figure 3 (A)). Figure 3 reveals that the UPL model can be fitted well with the real part of the conductivity spectra of P [VBTP][Cl] of PIL homopolymer, PIL copolymer and ion exchanged PIL copolymer.

3.5 | Ionic conductivity and relaxation time

Figure 4 reveals that the ionic conductivity which is the key factor for applications of the material, as obtained from the fitting of complex conductivity spectra, increased with the increase of temperature for each PIL system. It should be noted that the ionic conductivities of P[VBTP] [Cl] and different PIL samples (**P1** to **P9**) at 303 K are given in Table 2. As shown in Figure 4(A), the ionic conductivity of the PIL copolymers was high and increased with the increase of ionic content in these copolymers (**P1-P3**). It was also observed that the ionic conductivity of blend samples (**P8-P9**) was slightly lower than those of their corresponding copolymers (**P1** and **P3**) containing same ionic PIL content (Figure 4(A)). The cross-sectional FESEM images (Figure S17) of physical blend of P[VBTP] [Cl]/PMMA and P[VBTP][Cl]-*ran*-PMMA copolymer clearly revealed the heterogeneous phase separated structure for the former and homogeneous structure for the later. The phase separation in P[VBTP][Cl]/PMMA blend
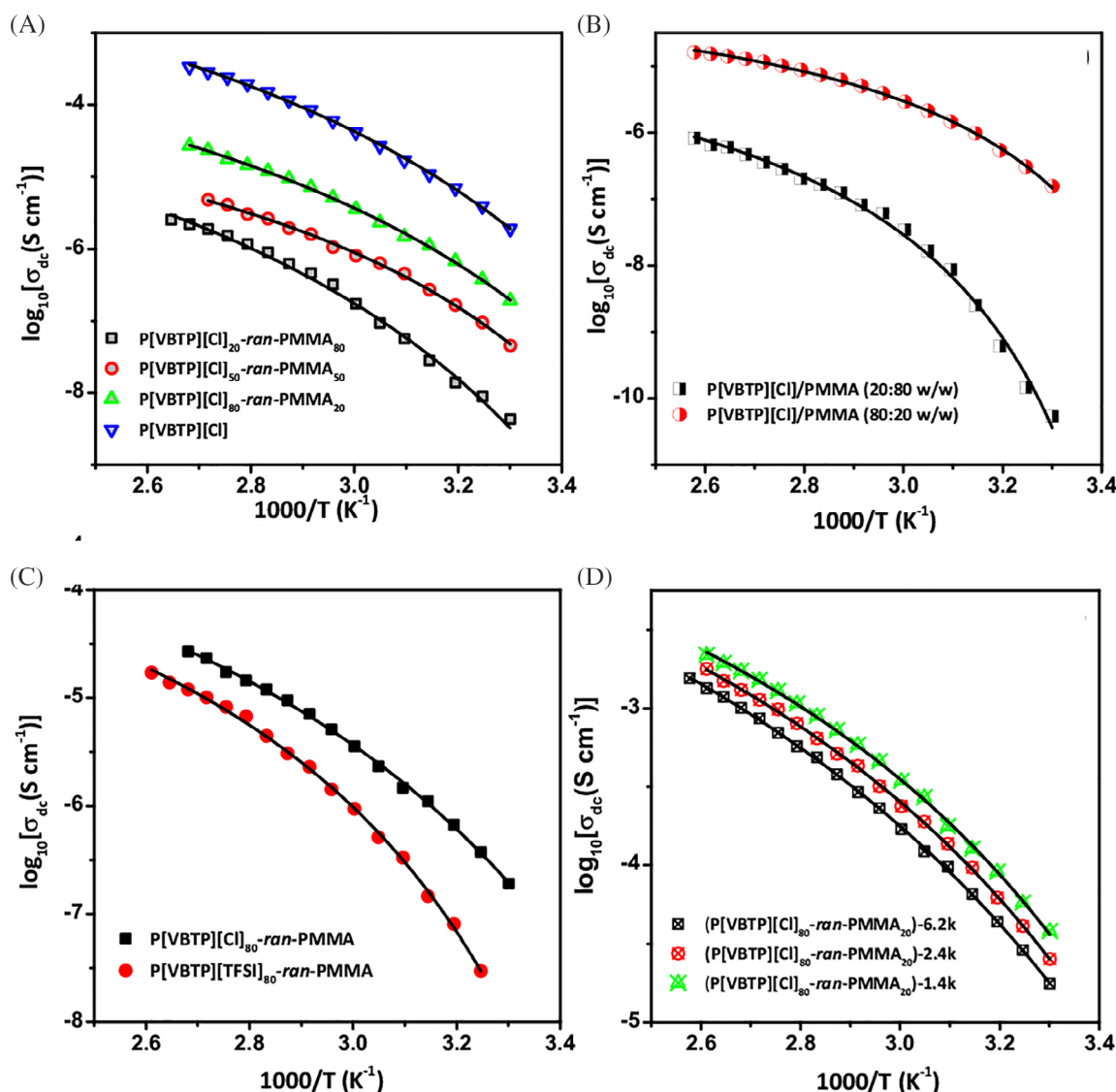

FIGURE 4 (A)–(D) Reciprocal temperature dependence of ionic conductivity, σ_{dc} for P[VBTP][cl] and different P[VBTP][cl] based systems. Solid black lines are best fits to VTF equation (Equation 2) [Color figure can be viewed at wileyonlinelibrary.com]

is attributable to the immiscibility of non-ionic PMMA and ionic P[VBTP][Cl] phases. It seems that the ionic P [VBTP][Cl] phase dispersed into the continuous PMMA matrix. The phase separation between ionic and non-ionic components lengthens the ion transport pathway, resulting in a lowering of the overall ionic conductivity in physically mixed ionic PIL/nonionic polymer system. Zhang and co-workers quantitatively established the correlation between ionic conductivity and extent of phase separation and observed that nano-scale phase separation rather than large micro or micro is more favorable to increase ionic conductivity.[62] In case of our materials, micro phase separation formed for PIL/PMMA (20:80 w/w), whereas for higher concentration of PIL and lower concentration of PMMA (PIL/PMMA [80:20 w/w]), ionic conductivity increases whose value is slightly lower than copolymer sample. The nanoscale phase separation in the blend films is probably the reason behind this observation. The values of ionic conductivity of **P4** copolymer (Table 2) with large-sized TFSI$^-$ anion showed lower value than that of PIL copolymer having same ionic content and small-sized Cl$^-$ anion (Figure 4(C)). It is reported that the PIL chains are better packed when larger size counter anions are present while frustrated chain packing is observed for smaller size of counter anions.[63] The frustrated chain packing causes more disorder structure and leads to lower the energy barrier for ion transport from one site to another via hopping. The existence of smaller Cl$^-$ anion in PIL copolymer (**P3**) leads to frustration chain packing compared to the corresponding large size TFSI$^-$ anion in **P4** copolymer.[63] However, there was a drastic increase of the ionic conductivity as the molecular weight (M_n) of PIL copolymer decreased from P[VBTP][Cl]-*ran*-PMMA-29 k to P[VBTP][Cl]-*ran*-PMMA-6.2 k (Table 2). When the decrease of molecular weight is less (PIL-*ran*-PMMA-6.2 k to PIL-*ran*-PMMA-1.4 k), the increase of conductivity was low. The enhancement of ionic conductivity with decrease of M_n occurred due to increase of ionic diffusivity which has been discussed later and ion motion becomes more correlated with structural relaxation at the same time.[64,65] It is also worth mentioning that the slight lower value of ionic content in **P6** and **P7** (Table 2) than that of PIL-ran-PMMA-6.2 k (**P5**) did not influence the ionic conductivity values significantly. The ionic conductivity value followed the increasing trend after changing the M_n from 6.2 k to 1.4 k value due to faster segmental dynamics in **P6** and **P7** than that of **P5**. Table 2 revealed that the value of power law exponent n at fixed temperature is almost independent of PIL and PIL related compositions and value of n lies between 0.54–0.65, indicating no change in correlation among PIL's compositional variation. Also, the average value of exponent $n \sim 0.57$ corresponds to a 3D conduction in the present PIL systems.[61]

Figure 4 shows that the temperature dependence of the ionic conductivity of PIL and PIL based systems exhibited the Vogel-Fulcher-Tammann (VTF) behavior,[66–68] which has also been applied to understand the dynamical process of the various glassy and polymeric systems and is given by:

$$\sigma_{dc}(T) = \sigma_0' T^{-1/2} \exp\left[\frac{-E_\sigma}{k_B(T - T_0)}\right] \quad (2)$$

where σ_0' is the pre-exponential factor, E_σ is the activation energy related to the critical free volume for ion transport and T_0 is the equilibrium Vogel scaling temperature. In this case, the σ_{dc} for all PILs and PIL copolymers has been fitted to Equation 2 according to nonlinear least square fits and the results are shown in Figure 4. The values of fitting parameters E_σ and T_0 are displayed in Table 3.

The reciprocal temperature dependence of inverse hopping time ($1/\tau_H$) of P[VBTP][Cl] obtained from UPL model and its copolymers were obtained from the best fits of conductivity data (Figure 5), which also obeyed VTF behavior, given by

$$\tau_H(T) = \tau_0 \exp\left[\frac{E_H}{k_B(T - T_0)}\right] \quad (3)$$

The values of VTF fitting parameters E_H and T_0', obtained from the best fits, are given in Table 3, which revealed that the fit parameters E_σ, E_H, T_0 and T_0' obtained from both σ' and τ_H are very close to each other, indicating a common conduction and relaxation mechanism in this PIL and its random PIL copolymers. The VTF fits indicated that the ion conduction and relaxation is coupled with polymer segmental motion contributing to the conductivity.

It has been observed that the increment of ionic content in PIL copolymers and lowering of molecular weight of PIL copolymers enhance the ionic conductivity. The size of counter ion and physical mixing of PIL and PMMA also influence the ionic conductivity. Ion conduction is also controlled by segmental motion of polymer chain. To analyze these effects, simultaneous determination of conducting ion number density and their diffusivity by using electrode polarization is more significant as mentioned below.

3.6 | Conducting ion diffusivity and number density

We have simultaneously determined the free ion diffusivity (D) and ion number density (P) from the theoretical model for EP, occurring at the low frequency region of

TABLE 3 The parameters obtained from the fitting of VTF relation to the temperature dependence of ionic conductivity σ_{dc}, hopping time τ_H and free mobile ion diffusivity D and also Arrhenius fitting parameters to ion number density (P) for several PIL based systems

PILs	Ionic conductivity		Hopping time		Ion diffusivity		Ion density	
	E_σ (eV) (±0.002)	T_0 (K) (±3)	E_H (eV) (±0.006)	T_0' (K) (±2)	E_D (eV) (±0.004)	T_0'' (K) (±4)	P_∞ (cm^{-3})	E_{dis} (meV) (±4)
P[VBTP][Cl]	0.025	224	0.031	223	0.022	235	1.6×10^{20}	65
P1	0.086	232	0.096	238	0.083	242	8.9×10^{18}	102
P2	0.065	238	0.062	234	0.073	231	1.2×10^{19}	90
P3	0.046	225	0.048	231	0.045	241	7.4×10^{19}	70
P4	0.049	252	0.054	240	0.061	243	4.2×10^{19}	86
P5	0.021	222	0.026	239	0.027	253	9.3×10^{20}	58
P6	0.018	218	0.021	235	0.021	243	1.1×10^{21}	53
P7	0.012	208	0.018	234	0.019	224	1.3×10^{21}	49
P8	0.095	250	0.11	255	0.094	227	6.9×10^{17}	124
P9	0.061	242	0.063	234	0.045	243	1.8×10^{19}	102
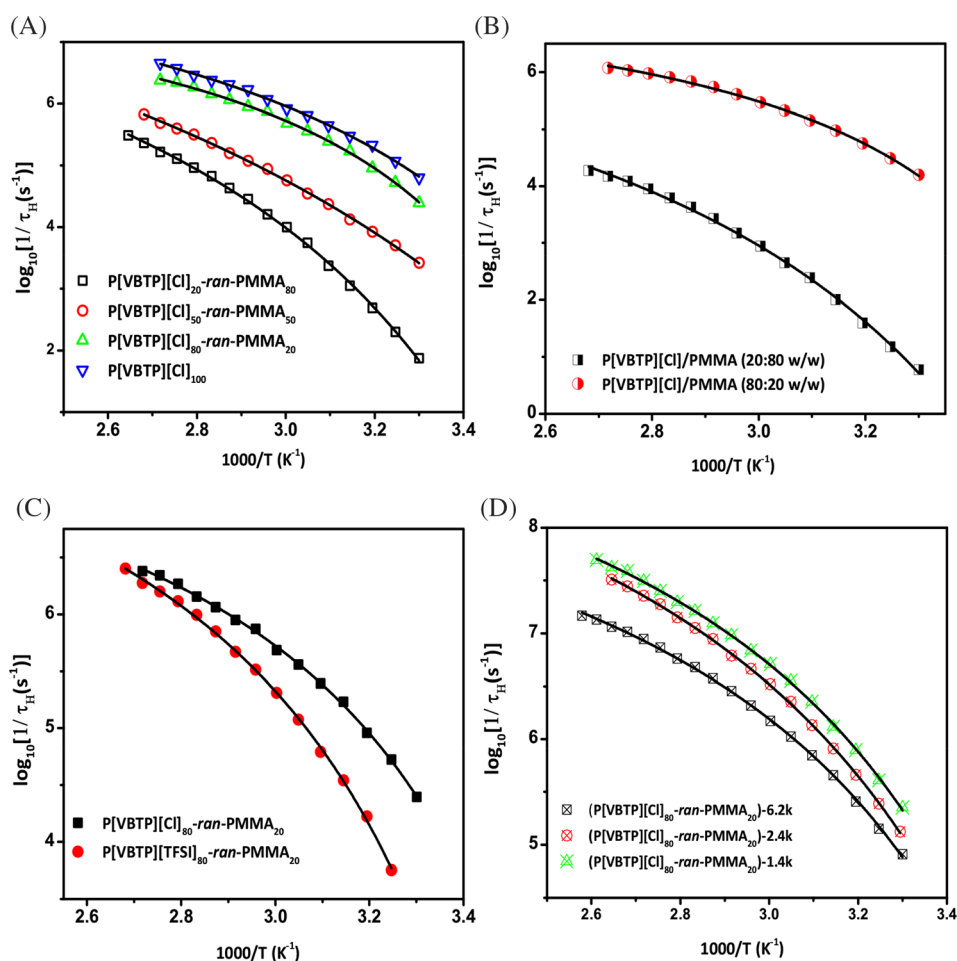
FIGURE 5 (A)–(D) reciprocal temperature dependence of relaxation time $\tau_H(T)$ for PIL and different PIL copolymers. Solid black lines are the best fits to VTF equation (Equation 3) [Color figure can be viewed at wileyonlinelibrary.com]

the dielectric spectra due to growth of ions at near metal electrode-PIL interface.[28,69,70] According to Macdonald and Coelho model, the electrode polarization can be described by loss tangent ($tan\delta$), which is expressed below in terms of τ_σ and τ_{EP} as a simple case of Debye relaxation.[71,72]

$$\tan\delta = \frac{\omega\tau_{EP}}{1+\omega^2\tau_\sigma\tau_{EP}} \qquad (4)$$

where ω is the angular frequency, $\tau_{EP}(=\varepsilon_{EP}\varepsilon_0/\sigma_{dc})$ is the response of full development of polarization of conducting ions at the low frequency region and $\tau_\sigma(=\varepsilon_s\varepsilon_0/\sigma_{dc})$ is time scale for ion conduction, when ion motion becomes diffusive as described above in Figure 2.[69] The loss tangent spectra for a representative sample, P[VBTP][TFSI]$_{80}$-*ran*-PMMA$_{20}$ at different temperatures are presented in Figure 6(A), where the solid black lines were obtained by fitting the data to Equation 4 for temperatures 308 K and 368 K. The peak of loss tangent ($tan\delta$) would usually occur at the geometric mean ($\omega = \tau_0^{-0.5}\tau_{EP}^{-0.5}$) of the τ_σ and τ_{EP} time scales.[16] For this sample, we observed that the $tan\delta$ peak shifted towards the higher frequency scale with increasing-

temperature. The Macdonald and Coelho model, thus, can be used to simultaneously determine the free ion diffusivity (D) and ion number density (P) by τ_σ and τ_{EP}, obtained from $tan\delta$ fits with the help of the following equations:

$$D = \frac{L^2\tau_\sigma}{4\tau_{EP}^2} \text{ and } P = \frac{1}{\pi l_B L^2}\left(\frac{\tau_{EP}^2}{\tau_\sigma}\right) \qquad (5)$$

where L is the sample thickness, l_B ($=e^2/4\pi\varepsilon_s\varepsilon_0 k_B T$) is the Bjerrum length, k_B is Boltzmann constant and T is absolute temperature.

The reciprocal temperature dependence of ion diffusivity for different PIL-based systems is given in Figures 6 (B)-(D). It can be observed from Figure 6 that the ion diffusivity, D obeys the VTF behavior because D is controlled by polymer segmental motion and is expressed by the following equation:

$$D = D_\alpha \exp\left(\frac{-E_D}{k_B\left(T - T_0''\right)}\right) \qquad (6)$$

where D_∞ and T_0'' are the infinite temperature diffusivity and Vogel temperature respectively and E_D is the activation energy for the ion diffusivity. The solid black lines were the best fitted lines to Equation 6 (Figures 6(B)-(D)), and the fitting parameters are listed in Table 3. It is
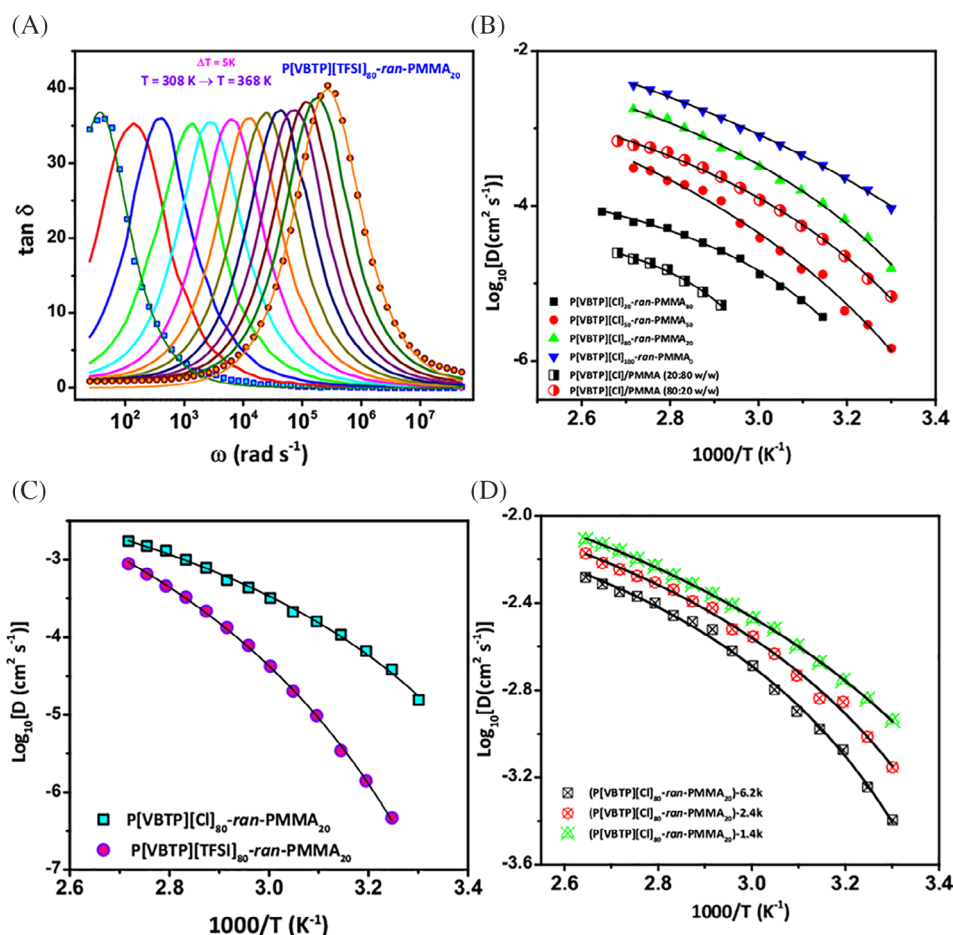
FIGURE 6 (A) A representative plot of angular frequency dependence of tan δ for P[VBTP][TFSI]$_{80}$-*ran*-PMMA$_{20}$ PIL (P4) at several temperatures and solid lines in Figure 6(A) for temperature 308 K and 368 K are fits to Equation 4, (B), (C) and (D) reciprocal temperature dependence of diffusivity, D obtained from Macdonald-Coelho model for different P[VBTP][Cl] copolymers, physical mixture of P[VBTP][Cl] and PMMA systems, TFSI-based PIL copolymer and P[VBTP][Cl] copolymers of different M_n [Color figure can be viewed at wileyonlinelibrary.com]

noted that the values of VTF fitting parameters for diffusivity were close to those obtained from the fits of σ_{dc} as well as τ_H. Thus, it can be concluded that the ion transport and relaxation were coupled with the polymer segmental motion and obeyed a common fundamental mechanism. Further, the ion diffusivity of different P[VBTP][Cl] copolymers increased with the increase of ionic PIL content in copolymer, while the ion diffusivity decreased when P[VBTP][Cl] was physically mixed with PMMA (Figure 6(C)). Figure 6(C) shows that the diffusivity of free conducting TFSI$^-$ ion decreased in P[VBTP][TFSI]$_{80}$-ran-PMMA$_{20}$ in comparison to that of Cl$^-$ anion in P[VBTP][Cl]$_{80}$-ran-PMMA$_{20}$ PIL due to comparatively larger size of TFSI$^-$ ion. The enhancement of ion diffusivity (mobility) with lowering the molecular weight of PILs can also be clearly seen from Figure 6(D). As per the earlier report, the ion transport (diffusivity) is directly linked with polymer segmental motion (structural relaxation) and the segmental motion increases with the decrease of molecular weight of PILs. Therefore, our result matched with what was reported earlier.[64]

The reciprocal temperature dependence of ion number density P for different PIL systems is presented in Figure 7. The data clearly shows that the value of P increased with the increase of temperature. However, the number density followed a linear Arrhenius behavior at low temperature, which can be expressed as:

$$P = P_a \exp\left(\frac{-E_{dis}}{k_B T}\right) \tag{7}$$

where P_∞ and E_{dis} correspond to the total ion number density at infinite temperature ($T \to \infty$) and the dissociation energy. Figure 7 also indicated that the ion number density increased with the increase of ionic content in PIL copolymers (**P1**-**P3**), while its values were relatively lower for physical blends of P[VBTP][Cl]/PMMA (**P8** and **P9**). It is also worthy to note that the TFSI$^-$ ion number density in P[VBTP][TFSI]$_{80}$-ran-PMMA$_{20}$ is lower than that of Cl$^-$ anion in P[VBTP][Cl]$_{80}$-ran-PMMA$_{20}$ due to larger size of TFSI$^-$ anion. On the other hand, number density increased with the decrease of molecular weight of the PIL copolymers (**P5**-**P7**). The number of ions that contribute to the conductivity in each of these PIL systems at any given instant is thus consistent with the variation of ionic conductivity. The values of P_∞ and E_{dis} were obtained from the Arrhenius fits of the data shown in Figure 7 and the fitting parameters are listed in Table 3. It can be seen from Table 3 that the largest value of E_{dis} was observed for P[VBTP][TFSI]$_{80}$-ran-PMMA$_{20}$ in comparison to that of P[VBTP][Cl]$_{80}$-ran-PMMA$_{20}$ due to the large size of the TFSI$^-$ anion.
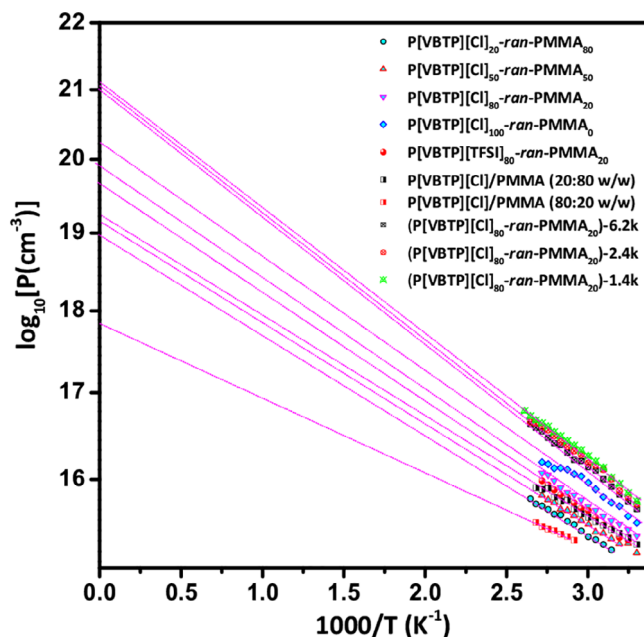

FIGURE 7 Reciprocal temperature dependence of free ion number density of different PIL based systems with the linear region at low temperature extrapolated to infinite temperature [Color figure can be viewed at wileyonlinelibrary.com]

It is worth mentioning that PIL and PIL based materials have been developed enormously to understand some fundamental aspects of their ion transport and relaxation mechanism, but a question about the applications of these materials are still a challenge for the materials scientists. Recently, Peltekoff and co-workers[73] fabricated thin-film transistors (TFTs) by using the very similar type of copolymers (P[VBBI$^+$TFSI$^-$-ran-MMA]) forming an electric double-layer (EDL) resulted in n-type TFT devices. More recently, Zhang and co-workers[62] demonstrated an alternating strategy to obtain solid polymer electrolytes having high mechanical strength, high ionic conductivity, high electrochemical stability and less Li dendrites growth by blending of copolymer based PIL (PPaB-MT) and P(VdF-HFP) containing 20% LiTFSI salt for Li-ion batteries. Cai and co-workers[74] also synthesized PIL based quasi-solid-state copolymers (PEGDA-P(BA-co-[EVIm]TFSI) QPE-IL) for lithium-sulfur batteries. Safa and coworkers[75,76] also synthesized a PIL (PDADMATFSI) based composite gel polymer electrolytes (PIL-EMIMTFSI-1 M LiTFSI) for lithium metal batteries (LMB). In this context, we have investigated the physicochemical properties such as thermal stability, moisture sensitivity and ion transport properties to know the applicability of our PIL based materials in energy storage applications. A comparison of such properties of some of the recently reported PILs and PIL based random copolymers along with our recent work is presented in Table 4.

TABLE 4   A comparison of decomposition temperature, moisture content, ionic conductivity of some of the recently reported PILs and PIL based random copolymers

PILs and PIL copolymers	Decomposition temperature (T_d) (°C)	Moisture content (wt%)	Ionic conductivity (S cm^{-1})	References
Poly(VBBI$^+$TFSI$^-$-ran-MMA)-34.4	-	-	1.6×10^{-9}	73
Poly(MMA-r-MEBIm-TFSI-15.4)	268	-	2.5×10^{-9} @ 383 K	77
PIL-copolymer (PPaB-MT)	~270	-	-	62
Poly(HMA-co-MEBIm-BF$_4$)-34.5 mol% HMA	~300		~2.5×10^{-6} @ 360 K	43
Poly(MEBIm-TFSI-co-MEBIm -BF$_4$)-32.8 mol% TFSI	~350	-	~1×10^{-5} @ 360 K	43
Poly-EGIm TFSI	278	-	3.9×10^{-7} @ 300 K	1
SBMIm poly-SEM	260	13.8	2.5×10^{-5} @ 300 K	1
P[C$_{18}$Vim][Br]	~290	-	~5×10^{-8} @ 298 K	34
[PS-TAC][Cl]	-	-	~1×10^{-8} @ 303 K	14
P[VBTP][Cl]	301	12.8	1.96×10^{-6} @ 303 K	This work
P[VBTP][Cl]$_{80}$-ran-PMMA$_{20}$	316	6.41	1.95×10^{-7} @ 303 K	This work
P[VBTP][TFSI]$_{80}$-ran-PMMA$_{20}$	365	1.84	2.96×10^{-8} @ 303 K	This work
P[VBTP][Cl]$_{80}$-ran-PMMA$_{20}$-1.4 k	265	10.45	3.73×10^{-5} @ 303 K	This work

As observed from Table 4 that PIL and PIL based random copolymers reported in present work showed good thermal stability, less moisture sensitivity and good ionic conductivity and that fundamental view ensures the potential use of these materials as polymer electrolytes in energy storage devices.

4 | CONCLUSIONS

In this report, a series of poly(ionic liquid) random copolymers comprising of ionic PIL and non-ionic PMMA segments were synthesized by using both free radical polymerization as well as reversible addition-fragmentation chain-transfer (RAFT) polymerization methods. The influence of copolymer compositions, counter anions (Cl$^-$ and TFSI$^-$) and molecular weight as well as physical mixing of copolymer segments on ion transport and relaxation were investigated using broadband dielectric spectroscopy followed by analyzing the data using a theoretical model. The free ion diffusivity

and ion number density of these random copolymers were obtained by analyzing the contribution of electrode polarization. The temperature dependence of ionic conductivity, relaxation time and ion diffusivity exhibited Vogel-Tammann-Fulcher behavior in these copolymers indicating ion transport controlled by segmental motion. With increasing ionic content of PIL, the ionic conductivity increased in the random copolymers. P[VBTP][Cl]$_{80}$-ran-PMMA$_{20}$ copolymer showed the ionic conductivity of 1.95×10^{-7} S cm^{-1} while the neat P[VBTP][Cl] exhibited the high ionic conductivity of 1.96×10^{-6} S cm^{-1} at room temperature. In spite of low ionic conductivity, the applicability of PIL copolymers as energy storage materials are higher because of their less moisture sensitivity due to incorporation of hydrophobic PMMA segment. The ionic conductivity decreased due to the introduction of larger counter anion TFSI$^-$ in the place of Cl$^-$ ion in copolymer. Ionic conductivity increased with decreasing molecular weight. The random PIL copolymers showed a better thermal stability and a faster ion transport (ion diffusion) compared to physically mixing of two

homopolymers. In comparison with other reported systems (Table 4), these PIL copolymers with good thermal stability, less moisture sensitivity and good ionic conductivity are more attractive materials for energy storage applications.

CONFLICT OF INTEREST
The authors declare no competing financial interest.

DATA AVAILABILITY STATEMENT
The supporting data of this study are available in the supplementary material of this article.

ORCID
Tarun K. Mandal https://orcid.org/0000-0003-1626-8637

REFERENCES
[1] Z. Wojnarowska, H. Feng, M. Diaz, A. Ortiz, I. Ortiz, J. Knapik-Kowalczuk, M. Vilas, P. Verdía, E. Tojo, T. Saito, E. W. Stacy, N.-G. Kang, J. W. Mays, D. Kruk, P. Wlodarczyk, A. P. Sokolov, V. Bocharova, M. Paluch, *Chem. Mater.* **2017**, *29*, 8082.

[2] M. Armand, F. Endres, D. R. MacFarlane, H. Ohno, B. Scrosati, *Nat. Mater.* **2009**, *8*, 621.

[3] W. Xu, *Science* **2003**, *302*, 422.

[4] K. Nakamura, K. Fukao, T. Inoue, *Macromolecules* **2012**, *45*, 3850.

[5] B. Yu, S. P. O. Danielsen, A. L. Patterson, E. C. Davidson, R. A. Segalman, *Macromolecules* **2019**, *52*, 2560.

[6] C. R. Bridges, M. J. Ford, E. M. Thomas, C. Gomez, G. C. Bazan, R. A. Segalman, *Macromolecules* **2018**, *51*, 8597.

[7] I. Osada, H. de Vries, B. Scrosati, S. Passerini, *Angew. Chem., Int. Ed.* **2016**, *55*, 500.

[8] T. Y. Kim, H. W. Lee, M. Stoller, D. R. Dreyer, C. W. Bielawski, R. S. Ruoff, K. S. Suh, *ACS Nano* **2011**, *5*, 436.

[9] P. K. Singh, K.-I. Kim, N.-G. Park, H.-W. Rhee, *Macromol. Symp.* **2007**, *249-250*, 162.

[10] S. Sen, S. E. Goodwin, P. V. Barbará, G. A. Rance, D. Wales, J. M. Cameron, V. Sans, M. Mamlouk, K. Scott, D. A. Walsh, *ACS Appl. Polym. Mater.* **2021**, *3*, 200.

[11] R. J. Miller, V. M. Smith, S. A. Love, S. M. Byron, D. S.-D. La Cruz, K. M. Miller, *ACS Appl. Polym. Mater* **2021**, *3*, 1097.

[12] E. W. Stacy, C. P. Gainaru, M. Gobet, Z. Wojnarowska, V. Bocharova, S. G. Greenbaum, A. P. Sokolov, *Macromolecules* **2018**, *51*, 8637.

[13] C. Iacob, A. Matsumoto, M. Brennan, H. Liu, S. J. Paddison, O. Urakawa, T. Inoue, J. Sangoro, J. Runt, *ACS Macro Lett.* **2017**, *6*, 941.

[14] P. J. Griffin, J. L. Freyer, N. Han, N. Geller, X. Yin, C. D. Gheewala, T. H. Lambert, L. M. Campos, K. I. Winey, *Macromolecules* **2018**, *51*, 1681.

[15] C. Gainaru, E. W. Stacy, V. Bocharova, M. Gobet, A. P. Holt, T. Saito, S. Greenbaum, A. P. Sokolov, *J. Phys, Chem. B* **2016**, *120*, 11074.

[16] C. Karlsson, P. Jannasch, *ACS Appl. Energy Mater.* **2019**, *2*, 6841.

[17] N. S. Schauser, R. Seshadri, R. A. Segalman, *Mol. Syst. Des. Eng.* **2019**, *4*, 263.

[18] F. Fan, W. Wang, A. P. Holt, H. Feng, D. Uhrig, X. Lu, T. Hong, Y. Wang, N.-G. Kang, J. Mays, A. P. Sokolov, *Macromolecules* **2016**, *49*, 4557.

[19] F. Fan, Y. Wang, T. Hong, M. F. Heres, T. Saito, A. P. Sokolov, *Macromolecules* **2015**, *48*, 4461.

[20] M. A. Ratner, D. F. Shriver, *Chem. Rev.* **1988**, *88*, 109.

[21] J.-P. Hansen, I. R. McDonald, *Theory of Simple Liquids : With Applications to Soft Matter.* 4, New York: Academic Press; **2013**.

[22] P. G. Wolynes, *Annl. Rev. Phys. Chem.* **1980**, *31*, 345.

[23] M. G. McLin, C. A. Angell, *Solid State Ionics* **1992**, *53-56*, 1027.

[24] M. A. Ratner, P. Johansson, D. F. Shriver, *MRS Bull.* **2000**, *25*, 31.

[25] J. B. Boyce, B. A. Huberman, *Phys. Rep.* **1979**, *51*, 189.

[26] S. Hull, *Rep. Prog. Phys.* **2004**, *67*, 1233.

[27] Y. Wang, A. L. Agapov, F. Fan, K. Hong, X. Yu, J. Mays, A. P. Sokolov, *Phys. Rev. Lett.* **2012**, *108*, 088303.

[28] U. H. Choi, Y. Ye, D. Salas de la Cruz, W. Liu, K. I. Winey, Y. A. Elabd, J. Runt, R. H. Colby, *Macromolecules* **2014**, *47*, 777.

[29] M. Lee, U. H. Choi, R. H. Colby, H. W. Gibson, *Chem. Mater.* **2010**, *22*, 5814.

[30] E. U. Mapesa, M. Chen, M. F. Heres, M. A. Harris, T. Kinsey, Y. Wang, T. E. Long, B. S. Lokitz, J. R. Sangoro, *Macromolecules* **2019**, *52*, 620.

[31] X. Luo, H. Liu, S. J. Paddison, *ACS Appl. Polym. Mater.* **2021**, *3*, 141.

[32] C. M. Evans, C. R. Bridges, G. E. Sanoja, J. Bartels, R. A. Segalman, *ACS Macro Lett.* **2016**, *5*, 925.

[33] K. Nakamura, T. Saiwaki, K. Fukao, *Macromolecules* **2010**, *43*, 6092.

[34] Y. Biswas, P. Banerjee, T. K. Mandal, *Macromolecules* **2019**, *52*, 945.

[35] U. H. Choi, R. H. Colby, *Macromolecules* **2017**, *50*, 5582.

[36] U. H. Choi, T. L. Price, D. V. Schoonover, R. Xie, H. W. Gibson, R. H. Colby, *Macromolecules* **2020**, *53*, 10561.

[37] J. C. Dyre, P. Maass, B. Roling, D. L. Sidebottom, *Rep. Prog. Phys.* **2009**, *72*, 046501.

[38] P. Pal, A. Ghosh, *J. Appl. Phys.* **2019**, *126*, 135102.

[39] K. Nakamura, K. Fukao, *Polymer* **2013**, *54*, 3306.

[40] A. I. Abdulahad, C. Jangu, S. T. Hemp, T. E. Long, *Macromol. Symp.* **2014**, *342*, 56.

[41] Y. Biswas, T. Maji, M. Dule, T. K. Mandal, *Polym. Chem.* **2016**, *7*, 867.

[42] W. Qian, J. Texter, F. Yan, *Chem. Soc. Rev.* **2017**, *46*, 1124.

[43] H. Chen, J.-H. Choi, D. Salas-de la Cruz, K. I. Winey, Y. A. Elabd, *Macromolecules* **2009**, *42*, 4809.

[44] S. Zhang, J. Runt, J. Phys, *Chem. B* **2004**, *108*, 6295.

[45] M. Wubbenhorst, J. van Turnhout, J. Non-Crysta, *Solids* **2002**, *305*, 40.

[46] P. Pal, A. Ghosh, *Phys. Rev. E* **2015**, *92*, 062603.

[47] A. A. Khamzin, I. I. Popov, R. R. Nigmatullin, *Phys. Rev. E* **2014**, *89*, 032303.

[48] A. Serghei, M. Tress, J. R. Sangoro, F. Kremer, *Phys. Rev. B* **2009**, *80*, 184301.

[49] J. Pitawala, J. Scheers, P. Jacobsson, A. Matic, J. Phys, *Chem. B* **2013**, *117*, 8172.

[50] J. R. Sangoro, C. Iacob, A. Serghei, C. Friedrich, F. Kremer, *Phys. Chem. Chem. Phys.* **2009**, *11*, 913.

[51] T. S. Sorensen, V. Compan, *J. Chem. Soc., Faraday Trans.* **1995**, *91*, 4235.

[52] M. E. Trukhan, *Sov. Phys. Solid State* **1963**, *4*, 2560.

[53] A. Munar, A. Andrio, R. Iserte, V. Compan, J. Non-Cryst, *Solids* **2011**, *357*, 3064.

[54] Y. Wang, F. Fan, A. L. Agapov, T. Saito, J. Yang, X. Yu, K. Hong, J. Mays, A. P. Sokolov, *Polymer* **2014**, *55*, 4067.

[55] U. H. Choi, M. Lee, S. Wang, W. Liu, K. I. Winey, H. W. Gibson, R. H. Colby, *Macromolecules* **2012**, *45*, 3974.

[56] W. Gorecki, M. Jeannin, E. Belorizky, C. Roux, M. Armand, *J. Phys. Condens. Matter* **1995**, *7*, 6823.

[57] D. P. Almond, A. R. West, *Nature* **1983**, *306*, 456.

[58] J. C. Dyre, *J. Appl. Phys.* **1988**, *64*, 2456.

[59] D. Feldman, *J. Polym. Sci., Polym. Lett. Ed.* **1988**, *26*, 371.

[60] A. K. Jonscher, *Nature* **1977**, *267*, 673.

[61] D. L. Sidebottom, *Phys. Rev. Lett.* **1999**, *83*, 983.

[62] M. Zhang, Q. Zuo, L. Wang, S. Yu, Y. Mai, Y. Zhou, *Chem. Commun.* **2020**, *56*, 7929.

[63] B. Doughty, A.-C. Genix, I. Popov, B. Li, S. Zhao, T. Saito, D. A. Lutterman, R. L. Sacci, B. G. Sumpter, Z. Wojnarowska, V. Bocharova, *Phys. Chem. Chem. Phys.* **2019**, *21*, 14775.

[64] J. R. Keith, S. Mogurampelly, F. Aldukhi, B. K. Wheatle, V. Ganesan, *Phys. Chem. Chem. Phys.* **2017**, *19*, 29134.

[65] S. Mogurampelly, J. R. Keith, V. Ganesan, *J. Am. Chem. Soc.* **2017**, *139*, 9511.

[66] H. Vogel, *Phys. Z.* **1921**, *22*, 645.

[67] G. Tammann, W. Hesse, *Z. Anorg. Allg. Chem.* **1926**, *156*, 245.

[68] G. S. Fulcher, *J. Am. Ceram. Soc.* **1925**, *8*, 339.

[69] R. J. Klein, S. Zhang, S. Dou, B. H. Jones, R. H. Colby, J. Runt, *J. Chem. Phys.* **2006**, *124*, 144903.

[70] D. Fragiadakis, S. Dou, R. H. Colby, J. Runt, *J. Chem. Phys.* **2009**, *130*, 064907.

[71] J. R. Macdonald, *Phys. Rev.* **1953**, *92*, 4.

[72] R. Coelho, *Rev. Phys. Appl. (Paris)* **1983**, *18*, 137.

[73] A. J. Peltekoff, V. E. Hiller, G. P. Lopinski, O. A. Melville, B. H. Lessard, *ACS Appl. Polym. Mater.* **2019**, *1*, 3210.

[74] X. Cai, B. Cui, B. Ye, W. Wang, J. Ding, G. Wang, *ACS Appl. Mater. Interface* **2019**, *11*, 38136.

[75] M. Safa, E. Adelowo, A. Chamaani, N. Chawla, A. R. Baboukani, M. Herndon, C. Wang, B. El-Zahab, *ChemElectroChem* **2019**, *6*, 3319.

[76] M. Safa, A. Chamaani, N. Chawla, B. El-Zahab, *Electrochim. Acta* **2016**, *213*, 587.

[77] Y. Ye, J.-H. Choi, K. I. Winey, Y. A. Elabd, *Macromolecules* **2012**, *45*, 7027.

SUPPORTING INFORMATION

Additional supporting information may be found online in the Supporting Information section at the end of this article.